Multilayer Multiconfiguration Time-Dependent Hartree Study on the Mode-/Bond-Specific Quantum Dynamics of Water Dissociation on Cu(111)

Qingfei Song, Xingyu Zhang, Fabien Gatti, Zekai Miao, Qiuyu Zhang, Qingyong Meng

Multi-Layer Multi-Configuration Time-Dependent Hartree Study on the Mode/Bond-Specific Quantum Dynamics of the Water Dissociation on Cu(111)

Qingfei Song,[1,2] Xingyu Zhang,[1] Fabien Gatti,[2,a)] Zekai Miao,[1] Qiuyu Zhang,[1,b)] and Qingyong Meng[1,c)]

[1)]*Department of Chemistry, Northwestern Polytechnical University, West Youyi Road 127, 710072 Xi'an, China*

[2)]*Institut des Sciences Moléculaires d'Orsay, CNRS-UMR 8214, Université Paris-Saclay, Bâtiment 520, F-91405 Orsay, France*

(Dated: 16 June 2022)

In this work, full dimensional (9D) quantum dynamics calculations on mode/bond-specific surface scattering of a water molecule on a copper (111) rigid surface are performed through the multilayer multiconfiguration time-dependent Hartree (ML-MCTDH) method. To easily perform the ML-MCTDH calculations on such triatomic molecule-surface system, we first choose specific Jacobi coordinates as set of coordinates of water. Next, to efficiently perform the 9D ML-MCTDH wavepacket propagation, the potential energy surface (PES) is transferred to canonical polyadic decomposition (CPD) form with the aid of a Monte Carlo based method. Excitation-specific dissociation probabilities of H_2O on Cu(111) are computed and mode/bond-specific dynamics are demonstrated by comparison with probability curve computed for a water molecule in ground state. The dependence of the dissociation probability of the initial state of H_2O is studied, and it is found that the excitation-specific dissociation probabilities can be divided into three groups. We find that the vibrationally excited states enhance the dissociation reactivity of H_2O, while the rotationally excited states hardly influence it.

Keywords: *H_2O/Cu(111)*; *ML-MCTDH*; *mode/bond-specific*; *canonical polyadic decomposition*

[a)]Electronic mail: fabien.gatti@universite-paris-saclay.fr

[b)]Electronic mail: qyzhang@nwpu.edu.cn

[c)]Electronic mail: qingyong.meng@nwpu.edu.cn

I. INTRODUCTION

Dissociative chemisorption of water on the metal surfaces was considered as an essential step in the steam reforming and the water-gas shift reaction. Figure 1 illustrates a total of nine coordinates $\mathbf{q}_9 = \{x, y, z, r_1, r_2, \theta_1, \theta_2, \phi, \alpha\}$ for the water molecule on a static metal-surface (say the copper surfaces), where $\{x, y, z\}$ is coordinates set of the center-of-mass (COM) of the water molecule and the other six coordinates represent the internal motions of the water molecule. Over the past decade, on the basis of reduced dimensional subsets of $\mathbf{q}_9$, several quantum-dynamics calculations on the H_2O/Cu(111) system have been reported. In 2012 Guo and co-workers[1] reported their six-dimension (6D) calculations on dissociative chemisorption of H_2O/Cu(111) system with a static surface, where the reduced model of $\mathbf{q}_6 = \mathbf{q}_9 \setminus \{x, y, \alpha\}$ in conjugation with the Chebyshev approach was used to propagate the nuclear wave function. These 6D calculations[1] predicted that excitations in all three vibrational modes of water are capable of enhancing reactivity more effectively than increasing translational energy, which is consistent with the late transition state (TS) in the reaction path according to the Polanyi rule[2–4]. Furthermore, Guo, Jiang, and co-workers extended the above 6D calculations on H_2O/Cu(111) to computationally describe state-to-state scattering of H_2O/Ni(111)[5].

On the other hand, based on their full-dimension (9D) potential energy surface (PES) constructed by neutral-network (NN), Zhang and co-workers[6–10] reported a series of reduced dimensional (6D and 7D) quantum dynamics calculations for the H_2O/Cu(111) system, where the reduced models of $\mathbf{q}_6 = \mathbf{q}_9 \setminus \{x, y, \alpha\}$ and $\mathbf{q}_7 = \mathbf{q}_9 \setminus \{x, y\}$ in conjugation with the split operator method was used. Moreover, the adiabatic sudden model for the in-plane coordinates was used to approximately simulate the 9D dissociation probability of H_2O/Cu(111) by extensive 7D dissociation probabilities at many impacting sites. Zhang and co-workers[8] found the largest enhancement of the asymmetric-stretching excitation among the excitations in all three vibrational modes of water. Moreover, Zhang and co-workers[6] also reported the 9D quantum dynamics calculations for H_2O/Cu(111), where the mode specificity was found to be controlled by the initial rovibrational eigen-states. Similar to the reduced dimensional calculations[1,7,8], Zhang and co-workers[6] again found that the enhancement of the excitation in asymmetric stretch is the largest which is similar to the reduced dimension results[1,7,8], while the bending mode is the smallest. Despite these fruitful dynamics results, all of previously reported calculations expanded the nuclear wave functions in the single-layer fashion, which is similar to the expansion of the electron wave function at the full

configuration interaction (full-CI) level. Hence, one can call such propagation scheme as CI-type methods. This also implies a rather high computational cost and thus limitation to higher dimensional calculations, that is, larger molecular reactions on the surfaces or including the motions of the atoms of the surface.

In this work, in order to effectively perform 9D quantum dynamics calculations, the multi-configuration time-dependent Hartree (MCTDH) together with its multi-layer version (ML-MCTDH) methods[11–17] are used to study the quantum dynamics of H_2O/Cu(111) on the basis of the NN PES constructed by Zhang and co-workers[6–9]. To this end, a new representation of the Hamiltonian operator is firstly constructed consistent with the MCTDH and ML-MCTDH methods which were originally designed for treating multi-dimension quantum dynamics. Special interest of the present calculations is taken on the dynamics dynamics initially promoted by various rovibrational excited states. The calculations in this work provide a comprehensive description of the vibrational quantum dynamics of H_2O/Cu(111). We also analyze the assignments of the first few excited vibrational modes. We begin with the kinetic energy operator (KEO) by dividing $\mathbf{q}_9$ into body-fixed and space-fixed subsets of coordinates, and then re-expressing the PES into the sum-of-product (SOP) form using the Monte Carlo algorithm. Having got both KEO and PES, we relax a guess wave function to the ground state using the improved-relaxation method[18], and then we compute the rovibrational excited states through the block-improved-relaxation (BLK) method[19] or the locked improved-relaxation method[18]. Based on these ro-vrationally excited states, extensive ML-MCTDH calculations are performed and then the propagated wave functions are analyzed to obtain the dissociation probability of water as a function of the collision energy. Note that MCTDH has already been used for other molecules on metal surfaces such as the H_2 dissociation[20] and to the CH_4 dissociation in reduced dimensionality[21] and to bimolecular scattering in gas phase[22–24]

The rest of this paper is organized as follows. In Section II, we will describe the present quantum dynamics calculations. Section III presents the numerical details, quantum dynamics results, and discussions. Finally, Section IV concludes with a summary.

II. THEORETICAL FRAMEWORK

A. Coordinates and Kinetic Energy Operator

Given in Figures 1 and 2 are definitions of the nine coordinates $\mathbf{q}_9 = \{x, y, z, r_1, r_2, \theta_1, \theta_2, \phi, \alpha\}$. The coordinates $\{x, y, z\}$ are the skewed Cartesian coordinates for the COM of water with respect to a laboratory-fixed (LF) frame linked to the metal surface, say the top atom. They correspond to the position of the origin of the space-fixed (SF) frame whose axes are parallel to the LF frame and whose origin is the COM of the water molecule. Thus, $\{x, y, z\}$ describe the global translation of the water molecule. The internal coordinates $\{r_1, r_2, \theta_1, \theta_2, \phi, \alpha\}$ represent the reactive motions of the water molecule. The r_1 coordinate is the length of the vector $\vec{r}_1$, which is the vector from the O atom to the H atom (see also Figure 1); r_2 the length of the vector $\vec{r}_2$, which is the vector from the COM of OH, G_{OH}, to the leaving H′ atom (see also Figure 1); θ_1 the angle between the $\vec{r}_1$ and $\vec{r}_2$ vectors. These three coordinates describe the deformation of the water molecule. The rest three coordinates $\{\theta_2, \phi, \alpha\}$ are the three Euler angles that describe the global rotation of the water molecule and the body-fixed (BF) frame with respect to the SF frame (see also Figure 1). The z axis of the BF frame, z^{BF}, is parallel to $\vec{r}_2$. The $(x^{\mathrm{BF}}, z^{\mathrm{BF}})$ half plan with $z \geq 0$ is definited such that $\vec{r}_1$ is parallel to this half plan. As illustrated in Figure 2, the nine coordinates $\{x, y, z, r_1, r_2, \theta_1, \theta_2, \phi, \alpha\}$ can be divided into three parts: (i) translational coordinates $\{x, y, z\}$ of the COM of H_2O, (ii) reactive coordinates $\{r_1, r_2, \theta_1\}$ of dissociation HOH′ → H′ + OH, and (iii) rotational coordinates $\{\theta_2, \phi, \alpha\}$ of H_2O.

The KEO for a set of two Jacobi vectors with our choice for the BF frame is well known[25,26]. This set of coordinates can be also seen as a trivial case of the general formulation of the so-called "polyspherical coordinates" that have been used many times successfully with MCTDH[27,28]. We have implemented the KEO in MCTDH according to Equation (35b) of Reference[27]. Since the nine coordinates are divided into three parts, it is easy to expect that the present KEO should be composed by three terms,

$$\hat{T} = \hat{T}_{\mathrm{COM}} + \hat{T}_{\mathrm{reax}} + \hat{T}_{\mathrm{rot}}. \tag{1}$$

The first term $\hat{T}_{\mathrm{COM}}$ means the KEO for the translational motions of the COM of H_2O. For the present H_2O/Cu(111) system, the x and y axes start from the top copper atom and point to the two nearest copper atoms with angle of 120° in the Cu(111) surface, while the z axis is perpendicular

to both x and y. Because of its skewed characteristic, $\hat{T}_{\mathrm{COM}}$ is given by

$$\hat{T}_{\mathrm{COM}} = -\frac{2}{3M}\left(\frac{\partial^2}{\partial x^2} + \frac{\partial^2}{\partial y^2} + \frac{\partial^2}{\partial x \partial y}\right) - \frac{1}{2M}\frac{\partial^2}{\partial z^2}, \tag{2}$$

where M is the total mass of the water molecule. Since the second and third terms usually coupled with each other, we consider them as a unified item $\hat{T}_{\mathrm{inner}} = \hat{T}_{\mathrm{reax}} + \hat{T}_{\mathrm{rot}}$. For the rotational coordinates of H_2O, $\{\theta_2, \phi, \alpha\}$, the KEO has a flexible form. Turning to θ_1, a flexible approach is necessary only if $\theta_1 = 0$ or $\theta_1 = \pi$. A semi-rigid form for θ_1 is adopted. Moreover, in order to have an hermitian conjugate momentum and non-Euclidean volume element

$$\mathrm{d}\mathcal{V} = \mathrm{d}r_1 \mathrm{d}r_2 \mathrm{d}u_1 \sin\theta_2 \mathrm{d}\theta_2 \mathrm{d}\phi \mathrm{d}\alpha, \tag{3}$$

we have used $u_1 = \cos\theta_1$ to construct $\hat{T}_{\mathrm{inner}}$ instead of θ_1 itself. Finally, according to Equation (35b) of Reference[27], the present KEO reads

$$\begin{aligned}
\hat{T} = & -\frac{2}{3M}\left(\frac{\partial^2}{\partial x^2} + \frac{\partial^2}{\partial y^2} + \frac{\partial^2}{\partial x \partial y}\right) - \frac{1}{2M}\frac{\partial^2}{\partial z^2} \\
& - \frac{1}{2}\sum_{i=1}^{2}\frac{1}{\mu_i}\frac{\partial^2}{\partial r_i^2} - \frac{1}{2}\left(\frac{1}{\mu_1 r_1^2} + \frac{1}{\mu_2 r_2^2}\right)\frac{\partial}{\partial u_1}(1-u_1^2)\frac{\partial}{\partial u_1} \\
& + \frac{1}{2}\left(\frac{1}{\mu_1 r_1^2} + \frac{1}{\mu_2 r_2^2}\right)\frac{\hat{J}_{z^{\mathrm{BF}}}^2}{1-u_1^2} + \frac{1}{2\mu_2 r_2^2}(\hat{J}^2 - 2\hat{J}_{z^{\mathrm{BF}}}^2) \\
& - \frac{1}{4\mu_2 r_2^2}\left(\frac{\partial}{\partial u_1}\sqrt{1-u_1^2} + \sqrt{1-u_1^2}\frac{\partial}{\partial u_1}\right)(\hat{J}_{+^{\mathrm{BF}}} - \hat{J}_{-^{\mathrm{BF}}}) \\
& + \frac{1}{4\mu_2 r_2^2}\frac{u_1}{\sqrt{1-u_1^2}}\Big[(\hat{J}_{+^{\mathrm{BF}}} + \hat{J}_{-^{\mathrm{BF}}})\hat{J}_{z^{\mathrm{BF}}} + \hat{J}_{z^{\mathrm{BF}}}(\hat{J}_{+^{\mathrm{BF}}} + \hat{J}_{-^{\mathrm{BF}}})\Big],
\end{aligned} \tag{4}$$

where $\mu_1 = m_{\mathrm{H}} m_{\mathrm{O}}/(m_{\mathrm{H}} + m_{\mathrm{O}})$ is the reduced mass associated with rotation of OH and $\mu_2 = m_{\mathrm{H}} m_{\mathrm{OH}}/(m_{\mathrm{H}} + m_{\mathrm{OH}})$ the reduced mass associated with dissociation $\mathrm{HOH}' \rightarrow \mathrm{H}' + \mathrm{OH}$. We refer the reader to Reference[27] for further technical details.

B. Dynamics Calculations

In the present work, we use the Heidelberg implementation[29] of the MCTDH algorithm[11,12,14,16,17], more precisely the multi-layer variant (ML-MCTDH)[30–33] for solving the time-dependent Schrödinger equation. These algorithms are well discussed in the literature[11,12,14,16,17,30–33], such that we only give a brief introduction here. Within the ML-MCTDH algorithm[30–33], the total time-dependent nuclear wave function is expressed in terms of a tensor in a hierarchical Tucker format which

has a tree-like structure (denoted by ML-tree), where the wave function is expanded in a set of multi-dimensional, time-dependent basis functions, called single particle functions (SPFs). The SPFs are themselves expanded in an underlying multi-dimensional, time-dependent basis functions. This expansion scheme is repeated until in the lowest level a time-independent primitive basis is used. The expansion relation between the l-th and $(l-1)$-th layers can be written as[32]

$$\varphi_m^{(\mathfrak{z}-1;\kappa_{l-1})}(Q_{\kappa_{l-1}}^{(\mathfrak{z}-1)},t)=\sum_{j_1}^{n_1^{(\mathfrak{z})}}\cdots\sum_{j_{p_{\kappa_l}}}^{n_{\kappa_l}^{(\mathfrak{z})}}A_{m;j_1,\cdots,j_{p_{\kappa_l}}}^{(\mathfrak{z})}(t)\prod_{\kappa_l=1}^{p^{(\mathfrak{z})}}\varphi_{j_{\kappa_l}}^{(\mathfrak{z},\kappa_l)}(Q_{\kappa_l}^{(\mathfrak{z})})=\sum_J A_{m;J}^{(\mathfrak{z})}\cdot\Phi_J^{(\mathfrak{z})}(Q_{\kappa_{l-1}}^{(\mathfrak{z}-1)}), \tag{5}$$

where $J=j_1,\cdots,j_p$, $\mathfrak{z}=\{l;\kappa_1,\cdots,\kappa_{l-1}\}$, and $\mathfrak{z}-1=\{l-1;\kappa_1,\cdots,\kappa_{l-2}\}$. The symbol l denotes the layer depth and $\mathfrak{z}$ indicates a particular node in the ML-tree. In order for saving computational cost, several physical coordinates with rather strong coupling can be combined to a logical coordinate, which can be further combined to the logical coordinates in deeper layer,

$$Q_{\kappa_{l-1}}^{(\mathfrak{z}-1)}=\{Q_1^{(\mathfrak{z})},\cdots,Q_{p_{\kappa_l}}^{(\mathfrak{z})}\}. \tag{6}$$

At the bottom layer the SPFs are to be replaced with time-independent primitive basis functions. By Equation (5), it is easy to find that the case of $l=1$ corresponds to the CI-type propagation method, while the case of $l=2$ corresponds to the MCTDH method with[11,12,14,16,17]. The structure of an multi-layer wavefunction is most conveniently visualized by a plot of the aforementioned tree structure. The tree used in the present work is shown in Figure 3.

Inserting the multi-layer *Ansätze* into the Dirac-Frenkel variational principle, the ML-MCTDH equations of motion (EOMs) for arbitrary layering schemes together with an algorithm for the recursive evaluation of all intermediate quantities entering the ML-MCTDH EOMs have been derived[30–33]. Noting the fact that MCTDH is a special case of ML-MCTDH with $l=2$, it is not surprising that the ML-MCTDH EOMs have a very similar structure to the MCTDH EOMs. For instance, the ML-MCTDH EOMs for the top layer coefficients are identical to the MCTDH ones,

$$i\frac{\partial A_{m;I}^{(1)}}{\partial t}=\sum_J\left\langle\Phi_I^{(1)}\middle|\hat{H}\middle|\Phi_J^{(1)}\right\rangle A_{m;J}^{(1)}=\sum_J\langle\hat{H}\rangle_{IJ}^{(1)}A_{m;J}^{(1)} \tag{7}$$

The ML-MCTDH EOM for the SPFs propagation are formally the same for all layers,

$$i\frac{\partial\varphi_n^{(\mathfrak{z},\kappa_l)}}{\partial t}=\left(1-P^{(\mathfrak{z},\kappa_l)}\right)\sum_{j,m}\left(\rho^{(\mathfrak{z},\kappa_l)}\right)_{nj}^{-1}\cdot\left\langle\hat{H}\right\rangle_{jm}^{(\mathfrak{z},\kappa_l)}\varphi_m^{(\mathfrak{z},\kappa_l)}, \tag{8}$$

where

$$P^{(\mathfrak{z},\kappa_l)}=\sum_j\left|\varphi_j^{(\mathfrak{z},\kappa_l)}\right\rangle\left\langle\varphi_j^{(\mathfrak{z},\kappa_l)}\right| \tag{9}$$

is the projector onto the space spanned by the SPFs $\varphi_j^{(\mathfrak{z},\kappa_l)}$, $\rho^{(\mathfrak{z},\kappa_l)}$ a density matrix and $\langle\hat{H}\rangle^{(\mathfrak{z},\kappa_l)}$ is a matrix of mean-field operators acting on the $\varphi_j^{(\mathfrak{z},\kappa_l)}$ functions. Mathematically, the ML-MCTDH EOMs are a set of coupled non-linear differential equations and can be efficiently solved using standard numerical tools[14,30–32]. In resolving the EOMs, one may choose *propagating* an initial eigen-state of the Hamiltonian operator using a real-valued time variable where the physical evolution of the system is simulated. To obtain the rovibrational eigen-state, an imaginary-valued time variable is used to *relax* a guess wave function, say improved relaxation[18] for ground state and BLK[19] for excited states.

C. Potential Energy Surface and its Canonical Polyadic Decomposition

As shown in Equations (7) and (8) the EOMs need extensive integrals for $\langle\hat{H}\rangle_{IJ}^{(l)}$ and $\langle\hat{H}\rangle^{(z,\kappa_l)}$. These integrals will be easily performed if $\hat{H}$ has an appropriate SOP form[14]. Since the KEO given in Equation (4) already has the SOP form (as always when using polyspherical coordinates), the PES must be further refitted to the SOP form. The PES used in the present work have been constructed by Zhang and co-workers[7,8], where a total of 93908 energy points were computed at the Perdew-Wang (PW91) level. In fitting the PES, a feed-forward NN model with two hidden layers was employed in conjugation with the NN structure of 9-85-75-1 where $\mathbf{q}_9$ is the inputs. The resulting 9D NN PES with the root mean square error (RMSE) of $\sim$ 10 meV indicates its accuracy. As a kind of SOP form, it was found[34,35] that the potential function in the canonical polyadic decomposition (CPD) form is more effective in performing the consequence ML-MCTDH calculations. In SOP or CPD form, the potential function is expanded by a series of the products of one-dimension function. This expansion is similar to the expansion of the nuclear wave function or SPFs (see also Equation (5)).

Generally, defining an appropriate set of grids, the CPD form of the f-dimensional potential function $V(q_1,\cdots,q_f)$ can be rewritten as[34,35]

$$V(q_1,\cdots,q_f) \simeq V^{(\mathrm{CPD})}(q_1,\cdots,q_f) = \sum_{r=1}^{R} c_r v_r^{(1)}(q_1)\cdots v_r^{(f)}(q_f), \tag{10}$$

where R is the expansion order, also called the rank of the CPD expansion ($R = 1024$ in this work), while $\{q_j\}_{j=1}^{f}$ are the set of f coordinates. The normalized basis functions $v_r^{(\kappa)}(q_\kappa)$ are often called the single-particle potentials (SPP), exclusively depend on only one coordinate. Using an underlying time-independent primitive basis, say basis functions of the discrete variable representation

(DVR)[14,36], the one-dimensional SPP function $v_r^{(\kappa)}(q_\kappa)$ can be replaced by its values evaluated on grid points, namely $v_{r,i_\kappa}^{(\kappa)} = v_r^{(\kappa)}(q_{\kappa,i_\kappa})$ for the i_κ-th grid point. Then, the multidimensional potential function in the CPD form $V^{(\mathrm{CPD})}$ is given in a tensors notation[34,35] on a set of grids,

$$V(\cdots, q_{\kappa,i_\kappa}, \cdots) \simeq V^{(\mathrm{CPD})}(\cdots, q_{\kappa,i_\kappa}, \cdots) = V_I^{\mathrm{CPD}} = \sum_r c_r \prod_\kappa v_{r,i_\kappa}^{(\kappa)} = \sum_r c_r \Omega_{r,I}, \tag{11}$$

where the multi-index $I = i_1, \cdots, i_f$ and the product $\Omega_{r,I} = \prod_\kappa v_{r,i_\kappa}^{(\kappa)}$ are introduced for clarity.

Having the potential values on the grids, V_I^{CPD}, the remaining task is to find both the expansion functions $\Omega_{r,I}$ and the coefficients c_r. To this end, the optimization target function for the κ-th coordinate is given by[34,35]

$$\mathcal{J}_\kappa = \sum_I W_I^{(\kappa)} \left(V_I - V_I^{\mathrm{CPD}}\right)^2 + \epsilon \sum_r c_r^2 \sum_I W_I^{(\kappa)} \Omega_{r,I}^2. \tag{12}$$

Introducing the index $I^\kappa = i_1, \cdots, i_{\kappa-1}, i_{\kappa+1}, \cdots, i_f$ which is the full combined index with the κth sub-index missing, a positive and coordinate-dependent weight function

$$W_I^{(\kappa)} = 1_\kappa \sum_{i_\kappa} W_I = 1_\kappa W_{I^\kappa}^{(\kappa)} \tag{13}$$

is defined, where the κ-th degree of freedom (DOF) has been integrated out and replaced by unity. On the one hand, the weight function will be used to emphasize regions of interest where increased fitting accuracy is required. For instance, the lower-lying energy regions where the wavefunction resides will be important during the reaction. On the other hand, the weight function will serve as a distribution function of sampling points when later the complete sum over I is replaced by Monte-Carlo sampling. Therefore, the first part of Equation (12) measures the difference of the CPD fit to the exact potential subject to the weight function. Moreover, ϵ is a regularization parameter, typically setting to square root of machine precision. Thus, the second part is called the regularization term. This part is introduced to penalize for (almost) linearly dependent terms in the CPD expansion, which may arise due to ill-conditioned matrices in the minimizing algorithm. We refer the reader to References[34,35] for further technical details on such Monte-Carlo sampled CPD transfermation technique that is called MCCPD.

III. RESULTS AND DISCUSSIONS

A. Numerical Details

To prepare the initial wave function, the water molecule is relaxed from a guess wave function to the rovibrational eigen-states (see also Section III B below) while the collision energy of the water molecule along the z coordinate has, as in all cases, been set to $p_z = -15.0$ au, such that H_2O travels towards the surface. To place the water molecule at some large enough distance of $z_0 = 6.0$ au from the surface when preparing $|\Psi_{\text{ro-vib}}\rangle$, we add an artificial harmonic potential with the force constant of $k = 10^{-2}$ au and a minimum at $z_0 = 6.0$ au to the z-coordinate and then compute the eigen-states of this augmented system Hamiltonian, keeping the surface as rigid. When the artificial harmonic potential is removed, the z-motion of water is no longer in an eigenstate but, after adding the initial momentum p_z, covers an energy range form zero to 0.25 eV. To this end, the initial wave function of the H_2O/Cu(111) system initially prepared as a product state

$$\Big|\Psi(t=0)\rangle = \exp(ip_z z)\Big|\Psi_{\text{ro-vib}}\rangle, \tag{14}$$

where $|\Psi_{\text{ro-vib}}\rangle$ is rovibrational eigen-state of the water molecule and the exponential term accounts for the initial momentum of H_2O towards the Cu(111) surface.

Given in Table I are primitive basis functions, namely basis functions of DVR, together with the number of the grid points and the range of the grids which are all used for representing the H_2O/Cu(111) system in the present dynamics calculations. The symbol of the one-dimension (1D) function for each coordinate for building the guess wave function in computing the rovibrational eigen-states as well as its parameters are also given in Table I. The parameters of the 1D wave functions include their positions and momenta, frequency ω_{HO} and mass M_{HO} of a harmonic oscillator (HO) function, width of a Gaussian function (*i.e.*, variance of the modulus-square of the Gaussian function) W_{GAUSS}, and the initial quantum numbers $(j_{\text{ini}}, m_{\text{ini}})$ of the angular 1D functions. In Table II, we give the numerical details of the present 9D MCCPD calculations, including the number of trajectory in Monte Carlo calculations and errors of the re-fitting calculations. The present 9D MCCPD calculation is carried out through a total of $\sim 7\times10^6$ Monte Carlo points. The resulting error of 7.49 meV in the MCCPD re-fitting together with the mean error of $\sim 10^{-3}$ meV imply that the present MCCPD calculations are accurate enough. Noting that the NN-PES of the H_2O/Cu(111) system was constructed with a fitting error of $\sim$ 10 meV[7,8], the present re-fitting errors are small enough to obtain reasonable results under the construction accuracy. Finally, the

primitive grids used in MCCPD are the same as the ones used in the ML-MCTDH calculations, as given in Table I. In MCCPD we also used the same mode combination scheme as for the wave function which is illustrated in Figure 3.

With the initial state prepared according to Equation (14) the water molecule will travel towards the Cu(111) surface where it may either be reflected and depart again or it is absorbed and sticks to the surface or it dissociates and sticks to the surface. The wave function of each initial state is propagate up to 10^3 fs by the ML-MCTDH method. To compute the sticking probability of the molecule or its fragments on the surface we analyse the flux of the wave function fraction through the surface positioned at $r_2^{(\mathrm{CAP})} = 4.0$ au. The dissociation probability is computed from the probability $P_{\mathrm{reax}}^{(r_2)}(E)$. To do this, beyond $r_2^{(\mathrm{CAP})}$ we place a complex absorbing potential (CAP)[37,38]

$$V_{\mathrm{CAP}}^{(r_2)} = -i\eta\Big(r_2 - r_2^{(\mathrm{CAP})}\Big)^n. \tag{15}$$

The CAP absorbs the reflected part of the wave packet if it reaches the region $r_2 \geq r_2^{(\mathrm{CAP})}$. In Equation (15), the quantities n and η are order and strength of the CAP along the r_2 coordinate, while $r_2^{(\mathrm{CAP})}$ marks the starting point of CAPs. In this work, we set $n = 3$ and $\eta = 0.05$ au. Furthermore, to prevent any reflow of population from the region of the CAP back towards the surface, we add a small artificial attractive potential that sucks a wave packet deeper into the CAP region. It is switched on after $t' = 120$ fs propagation time and at the position of $r_2 > r_2'$ with the form[35]

$$V_{\mathrm{att}}(r_2, t) = -a\vartheta(r_2 - r_2') \sin^3\left[\frac{\pi}{6}(r_2 - r_2')\right] \vartheta(t - t'), \tag{16}$$

where $a = 1.0 \times 10^{-3}$ au and $z' = 4.0$ au in this work. In Equation (16), ϑ is the Heaviside step function. For further technical details concerning the flux analysis we refer the reader to References[14,35,39,40]. In addition to flux analysis, the time-dependent expectation values of some observable quantity $A(t)$ are useful to obtain the dynamics. With the time-dependent wave function $\Psi(t)$ the expectation values $\langle A(t)\rangle$ have the form

$$\langle A(t)\rangle = \frac{\langle\Psi(t)\big|\hat{A}\big|\Psi(t)\rangle}{\langle\Psi(t)\big|\Psi(t)\rangle}, \tag{17}$$

where $\hat{A}$ is time-independent operator associated with $A(t)$. Moreover, when the time-dependent norms $\langle\Psi(t)|\Psi(t)\rangle$ become less than one, it is difficult to interpret the expectation values. This is because the CAP annihilates predominantly the fast-moving long-ranged parts of the wave functions. Therefore, only the expectation values at the beginning stage of scattering have capable to explain dynamics.

B. Eigen-States

In this work, the water molecule are prepared in the rovibrational eigen-states relaxed by 9D MCTDH calculations. Given in Table III are excitation energies of the H_2O/Cu(111) system for various modes with $z = 6.0$ au, as well as those of the water molecule in the gas phase for comparison. In Table III excitation energies (in cm^{-1}) of the water molecule in the first excited rovibrational states are given, where the bond symmetry and asymmetry stretches are denoted by ν_1 and ν_3, respectively, while the bond bending is denoted by ν_2. Based on these eigen-states, the mode-specific dynamics can be performed. It is worth to emphasize that, the angle θ_1 was transferred to u_1 in this work (see also Equation (4)) and thus the excitation of ν_2 will not be considered in the dynamics calculations. Indeed, according to the previous calculations by Zhang and co-workers[6], excitation of ν_2 hardly influence the dissociation probabiliy. To further consider the bond-specific dynamics, we also compute excitation energies for the vibrational excitations of the O-H bonds, ν_4 and ν_5, together with the frustrated rotations of the α, ϕ, and θ_2 (see also Figure 1) of the BF coordinates set (denoted by ν_6, ν_7, and ν_8, respectively). For comparison, excitation energies of the normal vibration modes of H_2O are also given in Table III, including those computed by resolving eigen-problem of the nuclear Hamiltonian operator, those computed by various electron structure calculations, and those measured by spectrum experiments.

As shown in Table III, the present excitation energies and those computed by Zhang and co-workers[6] are approximately identical with the differences are smaller than 10 cm^{-1}. It is not surprising if one remembers that we use the same PES as that used in the previous calculations[6]. Moreover, based on their own PES, Guo and co-workers[1] reported the vibrational excitation energies of H_2O/Cu(111), which are generally 100 cm^{-1} smaller than the present results. This may be caused by (i) tiny different of the shapes of the PESs used in these calculations and (ii) the reduced dimension in the calculations of Guo and co-workers[1]. Noting the fact that $100\,cm^{-1} \approx 12.4$ meV, point (i) is not surprising because these differences are roughly equal to the error in fitting PESs[1,6]. Turning to point (ii), in the reduced dimension scheme[1] three DOFs were ignored making the constraints on the normal model weaker and thus making frequencies of the normal modes smaller than those by full dimension calculations. On the other hand, all calculations predict that frequencies of the normal modes of H_2O/Cu(111) are smaller than those of H_2O in the gas phase. For example, frequency of the symmetry stretch (3520 cm^{-1}) is roughly 300 cm^{-1} smaller than that of H_2O in the gas phase at the CCSD(T) level. This might be raised from the existence of the Cu(111)

surface.

Finally, illustrated in Figure 4 are contour plots of the initial wave functions for the symmetry and asymmetry stretch modes together with those of the PES. By Figure 4 one can clearly find the symmetry or asymmetry feature of the stretch normal mode. It is clear that the symmetry mode (see the left panel of Figure 4) is the summation of the r_1 and r_2 bond stretches, while the asymmetry mode (see the right panel of Figure 4) is subtraction of the two bond stretches. Obviously, this is consistent with the group-theory analysis for the normal modes of H_2O. Moreover, in Figure 5 we also show the contour plots of the initial wave functions for bond-specific dynamics calculations. By the nodal planes of these contour plots various bond excitations can be clearly identified. The above calculations for excitation enegries and wave functions imply that the present 9D MCTDH relaxations are reasonable and accurate.

C. Mode/Bond-Specific Dynamics

With the various initial initial states as discussed in Section III B, extensive ML-MCTDH propagations and follow-up flux and expectation analyses are performed to compute the sticking probabilities and time-dependent expectation curves. Now, we shall show results obtained with the 9D Hamiltonian model for scattering off a rigid surface. Figure 6 displays the sticking probabilities as a function of the collision energies for the different initial states. In general, one observes that the dissociation probability curves are approximately equal to zero, when the impacting energy is less than roughly 0.15 eV. Moreover, at the impacting energy of more than 0.15 eV, the dissociation probability curves increase from zero to $10^{-3} \sim 10^{-2}$. To understand this feature of the flux analysis, the general features of the time-dependent expectation curves have to be given. Illustrated in Figure 7 are time-dependent expectation curves of the relative energy where the operator $\hat{A}$ in Equation (17) is $\hat{H} - E_0$ with $E_0 = E(t = 0)$ the total energy at $t = 0$. We also show the other expectation curves in the Supporting Information, including $\langle E(t)\rangle$, $\langle z(t)\rangle$, $\langle r_1(t)\rangle$, and $\langle r_2(t)\rangle$, where the operators are $\hat{H}$, $\hat{r}_1$, and $\hat{r}_2$, respectively. Here, we show expectation values only for times up to 450 fs, as the norms of wave functions become less than one for $t > 400$ fs (see also Figure 1 of the Supporting Information).

Turning to the dissociation probability curves computed by various initial-states (see colored lines in Figure 6), let us consider the mode- and bond-specific dynamics. The dissociation probability curves in Figure 6 can be clearly divided into three groups. The dissociation probability from

the symmetry excitation state (denoted by "symm. mode") itself composes a group with middle values and lowest value at the kinetic energy more than and less than 0.12 eV, respectively. The second group of dissociation probabilities contains those computed from the ground state (denoted by "GS") and the angular excitation states. The third group with larger values of dissociation probability is composed by those computed from the asymmetry excitation state (denoted by "asymm. mode") and the O-H bond excitation states (denoted by "r1 excitation" and "r2 excitation"). The reason why there are such three groups is directly that the mode/bond-excitations associated with the O-H bonds have capable to enhance the dissociation activity of the water molecule (as shown in Figures 4 and 5), but the excitations associated with the angular coordinates are not capable of this.

Indeed, for the rotational excited states, there is a small difference of the dissociation probabilities from the GS one and thus they compose the first group. Moreover, the excitations of the asymmetry mode as well as those for r_1 and r_2 enhance the reactivity of dissociation as these excitations associate with the reaction coordinate. Thus they belong to the second group. But, calculations from the excitation of the r_1 coordinate predict somewhat smaller values of the dissociation probability (see also the green line in Figure 6) due to the different settings of r_1 and r_2. Obviously, as illustrated by Figure 1, the dissociation coordinate mainly composed of r_2 coordinate instead of r_1 coordinate. Finally, excitation of the symmetry mode also enlarge the bond length values of the O-H bonds, it can thus enhance the dissociation probability. However, comparing with the second group, from state of excited symmetry mode ability to improve reactivity is not so large. Furthermore, at low energy lower than the dissociation barrier, excitation of the symmetric stretching vibration will not cause the dissociation of water, but will cause the molecules to tend to come back. This is because the movements of the two hydrogen atoms are in the same direction. These features of the symmetry excitation make its probability curve composes the third group alone. By Figure 6 we also note a crossing of the probability curves between the first and third groups at roughly 0.12 eV. Since the difference between these two probability curves are roughly 10^{-5}, which is too small to distinctly separate them. Therefore, we are supposed to say that they are equal to each other when the kinetic energy is less than roughly 0.12 eV.

Turning to the energy transfer on the rigid surface, let us consider the time-dependent expectation values of the relative energy as shown in Figure 7. When the water molecule approaches the Cu(111) surface, the relative energy is always equal to zero until $t = 160$ fs, implying the energy conservation during the dissociation. Near and slightly above $t = 300$ fs or $t = 400$ fs, the system

is transferred to another new state with energy conservation. It is also found that there exist a minimum along the curve computed from the excited states of the symmetry and asymmetry modes as well as O-H bond stretch, as shown by red, blue, green, and yellow lines in Figure 7. This might be caused by the energy rearrangement during the surface scattering of vibrationally excited water molecule.

D. Discussions

In 2012 Guo and Xie and co-workers[1] reported their quantum dynamics calculations on dissociative chemisorption of the H_2O/Cu(111) system with a static surface, where the Chebyshev approach was used to propagate the wave function. In their calculations[1], the mode selectivity of the symmetric stretching ν_1, bending ν_2, and antisymmetric stretching ν_3 modes of water in this dissociative chemisorption was examined on the 6D PES. They[1] found that excitations in all three vibrational modes are capable of enhancing reactivity more effectively than increasing translational energy, consistent with the late transition state in the reaction path. These results are consistent with the present results that the vibrational excitations of water play a central role in its dissociative chemisorption on Cu(111).

Later, to extend the 6D results to full dimensional case, Zhang and co-workers[6–10] first performed a series of reduced dimensional (6D and 7D) quantum dynamics calculations for the H_2O/Cu(111) system and its isotopic effects with static surface, where the split operator method was used to propagate the nuclear wave function. The 7D dissociation probabilities[7] at the TS, top, bridge, and hcp sites are quite different from the corresponding 6D probabilities with various fixed azimuthal angles α, indicating the great importance of the azimuthal angle. Through the sudden model for the in-plane modes as well as the site-average scheme, it is possible to approximate the 9D dissociation probability of H_2O on Cu(111) by 7D dissociation probabilities for many impacting sites. Later, Zhang and co-workers[8] found that excitations in all three vibrational modes of water have a significant impact on reactivity with the largest enhancement for the asymmetric-stretching excitation which are consistent with the present work. In 2016, the full dimension quantum dynamics calculations for H_2O/Cu(111) were reported by Zhang and co-workers[6], where the mode specificity was also considered by controlling the initial states as vibrational eigenstate. These calculations[6] predicted that the enhancement of the excitation in asymmetric stretch is the largest which is similar to the reduced dimension results[1,7,8] as well as the present results.

Finally, by their calculations, Zhang and co-workers[6] also predicted the importance of the lattice effects in dissociation chemisorption of H_2O/Cu(111). To consider the lattice effects, the expansion model for extending the PES has been proposed[35,39,41] the for the surface scattering of CO/Cu(100). For surface scattering of lighter molecule, such as H_2O/Cu(111), the expansion model is very suitable for considering its lattice effects. Under the expansion model, the surface atoms is vibrating around the equilibrium position $\mathfrak{Q}_0 = 0$ with small-amplitude. Thus, letting $\mathfrak{q}$ and $\mathfrak{Q}$ be coordinates sets of the molecule and the surface atoms, respectively, the whole potential energy $V(\mathfrak{q}, \mathfrak{Q})$ can be expanded into a Taylor series,[35,39,41]

$$\begin{aligned} V(\mathfrak{q}, \mathfrak{Q}) &= V^{(0)}(\mathfrak{q}, \mathfrak{Q}_0) + \sum_{j=1}^{N_{\text{grid}}} \sum_{\alpha=1}^{3} V_{j\alpha}^{(1)}(\mathfrak{q}) Q_{j\alpha} + \frac{1}{2} \sum_{j,k=1}^{N_{\text{grid}}} \sum_{\alpha,\beta=1}^{3} V_{j\alpha k\beta}^{(2)}(\mathfrak{q}) Q_{j\alpha} Q_{k\beta} + \cdots \\ &= V^{(0)}(\mathfrak{q}, \mathfrak{Q}_0) + \mathbf{V}^{(1)}(\mathfrak{q}) \cdot \mathfrak{Q} + \frac{1}{2} \mathfrak{Q}^{\dagger} \cdot \mathbf{V}^{(2)}(\mathfrak{q}) \cdot \mathfrak{Q} + \cdots , \end{aligned} \tag{18}$$

where $V^{(0)}(\mathfrak{q}, \mathfrak{Q}_0)$ denotes the potential function with all surface atoms fixed at their equilibrium positions. The sum in Equation (18) runs only over a selected set of surface atoms, the remaining surface atoms are still kept fixed at their equilibrium positions. Moreover, the series has to be truncated after some order, say the second order, keeping the computational effort manageable. By fitting each derivatives, one can then construct the PES with the coordinates of several surface atoms. Introducing the surface coordinates in the PES term, the KEO and PES of the clean surface should be directly added following the expression of Equation (11) of Reference[41]. Thus, use of the expansion model allows us to study the lattice effects which have been planned.

IV. CONCLUSIONS

In this work, full dimensional (9D) quantum dynamics calculations on mode/bond-specific surface scattering of a water molecule on the Cu(111) rigid surface are performed through the ML-MCTDH method. The PES was constructed by Zhang and co-workers[6–9] through NN fitting approach. Then, we derive the KEO by setting the Jacobi coordinates for the BF set of coordinates and introducing the angular coordinates to describe its relative orientations to the SF set of coordinates. To efficiently perform the 9D ML-MCTDH wavepacket propagation, the PES is further transferred to the CPD form with the aid of a Monte Carlo based method. Having the KEO and the PES in CPD, excitation-specific dissociation probabilities of H_2O on Cu(111) are computed by analysis of the propagated wave functions. Then, mode/bond-specific dynamics are demonstrated

by comparison with probability computed for ground state. To this end, extensive MCTDH relaxations are first performed. From these relaxed eigen-states, the dependence of the dissociation probability of the initial state of H_2O is studied. In this work, by extensive ML-MCTDH propagations, we find that the excitation-specific dissociation probabilities can be divided into three groups. Moreover, the vibrationally excited states enhance the dissociation reactivity of H_2O, while the rotationally excited states hardly influence it. The present results are consistent with the previous ones and the methodological framework introduced here opens the way to include the impact of a movable surface on the dynamics.

SUPPLEMENTARY MATERIAL

See Supplementary Material Documents at http://dx.doi.org/XXX for the definitions of the BF and SF frames of coordinates and the time-dependent expectation values.

ACKNOWLEDGEMENTS

Q.M. gratefully acknowledges financial support by National Natural Science Foundation of China (Grant No. 21773186) and Fundamental Research Funds for the Central Universities (Grant No. 3102017JC01001). Q.S. gratefully acknowledges Doctoral Dissertation Innovation Fund (Grant No. CX2021038) and China Scholarship Council (Grant No. 202106290145) for his visiting to Université Paris-Saclay. The authors thank the *Centre National de la Recherche Scientifique* (CNRS) International Research Network (IRN) "MCTDH" for financial support. The authors are very grateful to M. Schröder and H.-D. Meyer (Universität Heidelberg) for helpful discussions on MCCPD and ML-MCTDH and to T. Liu (Dalian Institute of Chemical Physics, Chinese Academy of Sciences) for providing the subroutine of the PES.

REFERENCES

[1]B. Jiang, J. Li, D. Xie, and H. Guo, "Enhancing dissociative chemisorption of H_2O on Cu(111) via vibrational excitation," Proc. Natl. Acad. Sci. U.S.A. **109**, 10224–10227 (2012).

[2]J. C. Polanyi and W. H. Wong, "Location of Energy Barriers. I. Effect on the Dynamics of Reactions A+BC," J. Chem. Phys. **51**, 1439–1450 (1969).

[3]J. C. Polanyi, "Some concepts in reaction dynamics (nobel lecture)," Angew. Chem. Int. Ed. **26**, 952–971 (1987).

[4]J. C. Polanyi and A. H. Zewail, "Direct observation of the transition state," Acc. Chem. Res. **28**, 119–132 (1995).

[5]B. Jiang and H. Guo, "Dynamics of water dissociative chemisorption on ni(111): Effects of impact sites and incident angles," Phys. Rev. Lett. **114**, 166101 (2015).

[6]Z. Zhang, T. Liu, B. Fu, X. Yang, and D. H. Zhang, "First-principles quantum dynamical theory for the dissociative chemisorption of h2o on rigid cu(111)," Nat. Commun. **7**, 11953 (2016).

[7]T. Liu, Z. Zhang, B. Fu, X. Yang, and D. H. Zhang, "A seven-dimensional quantum dynamics study of the dissociative chemisorption of h2o on cu(111): effects of azimuthal angles and azimuthal angle-averaging," Chem. Sci. **7**, 1840–1845 (2016).

[8]T. Liu, Z. Zhang, B. Fu, X. Yang, and D. H. Zhang, "Mode specificity for the dissociative chemisorption of h2o on cu(111): a quantum dynamics study on an accurately fitted potential energy surface," Phys. Chem. Chem. Phys. **18**, 8537–8544 (2016).

[9]T. Liu, Z. Zhang, J. Chen, B. Fu, and D. H. Zhang, "Mode specificity of the dissociative chemisorption of hod on rigid cu(111): an approximate full-dimensional quantum dynamics study," Phys. Chem. Chem. Phys. **18**, 26358–26364 (2016).

[10]T. Liu, B. Fu, and D. H. Zhang, "An approximate full-dimensional quantum dynamics study of the mode specificity in the dissociative chemisorption of d2o on rigid cu(111)," Phys. Chem. Chem. Phys. **19**, 11960–11967 (2017).

[11]H.-D. Meyer, U. Manthe, and L. S. Cederbaum, "The multi-configurational time-dependent Hartree approach," Chem. Phys. Lett. **165**, 73–78 (1990).

[12]U. Manthe, H.-D. Meyer, and L. S. Cederbaum, "Wave-packet dynamics within the multiconfiguration Hartree framework: General aspects and application to NOCl," J. Chem. Phys. **97**, 3199–3213 (1992).

[13]H.-D. Meyer, "Multiconfiguration time-dependent Hartree method," in *The Encyclopedia of Computational Chemistry*, Vol. 5, edited by P. v. R. Schleyer, N. L. Allinger, T. Clark, J. Gasteiger, P. A. Kollman, H. F. Schaefer III, and P. R. Schreiner (John Wiley and Sons, Chichester, 1998) pp. 3011–3018.

[14]M. H. Beck, A. Jäckle, G. A. Worth, and H.-D. Meyer, "The multi-configuration time-dependent Hartree (MCTDH) method: A highly efficient algorithm for propagating wave packets," Phys. Rep **324**, 1–105 (2000).

[15]H.-D. Meyer and G. A. Worth, "Quantum molecular dynamics: Propagating wavepackets and density operators using the multiconfiguration time-dependent Hartree (MCTDH) method," Theor. Chem. Acc. **109**, 251–267 (2003).

[16]H.-D. Meyer, F. Gatti, and G. A. Worth, eds., *Multidimensional Quantum Dynamics: MCTDH Theory and Applications* (Wiley-VCH, Weinheim, 2009).

[17]H.-D. Meyer, "Studying molecular quantum dynamics with the multiconfiguration time-dependent Hartree method," WIREs: Comput. Mol. Sci. **2**, 351–374 (2012).

[18]H.-D. Meyer, F. Le Quéré, C. Léonard, and F. Gatti, "Calculation and selective population of vibrational levels with the Multiconfiguration Time-Dependent Hartree (MCTDH) algorithm," Chem. Phys. **329**, 179–192 (2006).

[19]L. J. Doriol, F. Gatti, C. Iung, and H.-D. Meyer, "Computation of vibrational energy levels and eigenstates of fluoroform using the multiconfiguration time-dependent Hartree method," J. Chem. Phys. **129**, 224109 (2008).

[20]C. Crespos, H.-D. Meyer, R. C. Mowrey, and G. J. Kroes, "Multiconfiguration time-dependent Hartree method applied to molecular dissociation on surfaces: H_2+Pt(111)," J. Chem. Phys. **124**, 074706 (2006).

[21]G. P. Krishnamohan, R. A. Olsen, G.-J. Kroes, F. Gatti, and S. Woittequand, "Quantum dynamics of dissociative chemisorption of ch4 on ni(111): Influence of the bending vibration," J. Chem. Phys. **133**, 144308 (2010).

[22]R. Ellerbrock and U. Manthe, "Communication: Reactivity borrowing in the mode selective chemistry of H + CHD_3 → H_2 + CD_3," J. Chem. Phys. **147**, 241104 (2017).

[23]B. Zhao, U. Manthe, and H. Guo, "Fermi resonance controlled product branching in the h+ hod reaction," Phys. Chem. Chem. Phys. **20**, 17037 (2018).

[24]R. Ellerbrock and B. Z. nd U. Manthe, "Vibrational control of the reaction pathway in the $h+chd_3$ → h_2 + cd_3 reaction," Sciences advances **13**, eabm9820 (2022).

[25]B. T. Sutcliffe and J. Tennyson, "A generalized approach to the calculation of ro-vibrational spectra of triatomic molecules," J. Chem. Phys. **76**, 5710 (1982).

[26]B. T. Sutcliffe and J. Tennyson, "A generalized approach to the calculation of ro-vibrational spectra of triatomic molecules," Mol. Phys. **58**, 1053 – 1066 (1986).

[27]F. Gatti, C. Iung, C. Leforestier, M. Menou, Y. Justum, A. Nauts, and X. Chapuisat, "Vector parametrization of the three-atom problem in quantum mechanics," J. Mol. Struct. (Theochem) **424**, 181 (1998).

[28]F. Gatti and C. Iung, "Exact and constrained kinetic energy operators for polyatomic molecules: The polyspherical approach," Phys. Rep. **484**, 1–69 (2009).

[29]G. A. Worth, M. H. Beck, A. Jäckle, O. Vendrell, and H.-D. Meyer, The MCTDH Package, Version 8.2, (2000). H.-D. Meyer, Version 8.3 (2002), Version 8.4 (2007). O. Vendrell and H.-D. Meyer Version 8.5 (2013). Version 8.5 contains the ML-MCTDH algorithm. Current versions: 8.4.18 and 8.5.11 (2019). See http://mctdh.uni-hd.de/.

[30]H. Wang and M. Thoss, "Multilayer formulation of the multiconfiguration time-dependent Hartree theory," J. Chem. Phys. **119**, 1289–1299 (2003).

[31]U. Manthe, "A multilayer multiconfigurational time-dependent Hartree approach for quantum dynamics on general potential energy surfaces," J. Chem. Phys. **128**, 164116 (2008).

[32]O. Vendrell and H.-D. Meyer, "Multilayer multiconfiguration time-dependent Hartree method: Implementation and applications to a Henon-Heiles Hamiltonian and to pyrazine," J. Chem. Phys. **134**, 044135 (2011).

[33]H. Wang, "Multilayer Multiconfiguration Time-Dependent Hartree Theory," J. Phys. Chem. A **119**, 7951 (2015).

[34]M. Schröder, "Transforming high-dimensional potential energy surfaces into a canonical polyadic decomposition using Monte Carlo methods," J. Chem. Phys. **152**, 024108 (2020).

[35]Q. Meng, M. Schröder, and H.-D. Meyer, "High-dimensional quantum dynamics study on excitation-specific surface scattering including lattice effects of a five-atom surface cell," J. Chem. Theory Comput. **17**, 2702–2713 (2021).

[36]Z. Bačić and J. C. Light, Ann. Rev. Phys. Chem. **40**, 469 (1989).

[37]U. V. Riss and H.-D. Meyer, "Calculation of resonance energies and widths using the complex absorbing potential method," J. Phys. B **26**, 4503 (1993).

[38]U. V. Riss and H.-D. Meyer, "Investigation on the reflection and transmission properties of complex absorbing potentials," J. Chem. Phys. **105**, 1409 (1996).

[39]Q. Meng and H.-D. Meyer, "Lattice effects of surface cell: Multilayer multiconfiguration time-dependent Hartree study on surface scattering of CO/Cu(100)," J. Chem. Phys. **146**, 184305 (2017).

[40]A. Jäckle and H.-D. Meyer, "Time-dependent calculation of reactive flux employing complex absorbing potentials: General aspects and application within MCTDH," J. Chem. Phys. **105**, 6778 (1996).

[41]Q. Meng and H.-D. Meyer, "Expansion Hamiltonian model for a diatomic molecule adsorbed on a surface: Vibrational states of the CO/Cu(100) system including surface vibrations," J. Chem. Phys. **143**, 164310 (2015).

[42]G. Herzberg, *Molecular Spectra and Molecular Structure* (Krieger Pub Co, 1992).

TABLE I: The DVR-grids used in the present quantum dynamics calculations, and the one-dimension (1D) function in building the guess wave function in relaxations for rovibrational eigen-states. The definitions of the coordinates (indicated in the first column) are given in Figure 1. The second column describes the primitive basis functions, which underlay the DVR. The third column gives the number of the grid points in the present work. The fourth column gives the range of the grids in atomic unit or radian. The fifth column gives the symbol of the 1D function for each coordinate. The other columns give the parameters for these 1D functions, including positions and momenta in the 1D function, frequency ω_{HO} and mass M_{HO} of the 1D HO function, width of the GAUSS function W_{GAUSS}, and the initial quantum numbers $(j_{\mathrm{ini}}, m_{\mathrm{ini}})$ of the 1D angular functions.

Coordinates	Primitive basis function			Initial wave function			
	Symbol [a]	Grid points	Range of the grids	Symbol [b]	Position	Momentum	Parameters
x	EXP	27	[0.000, 4.830]	HO	2.415	0.000	$\omega_{\mathrm{HO}} = 16.500\ \mathrm{cm}^{-1}$, $M_{\mathrm{HO}} = 18.000$ AMU
y	EXP	27	[0.000, 4.830]	HO	2.415	0.000	$\omega_{\mathrm{HO}} = 16.500\ \mathrm{cm}^{-1}$, $M_{\mathrm{HO}} = 18.000$ AMU
z	FFT	128	[2.750, 9.000]	GAUSS	6.000	−15.000	$W_{\mathrm{GAUSS}} = 0.100$
r_1	HO	15	[1.000, 2.622] [c]	EIGENF	–	–	ground state
r_2	FFT	128	[1.300, 4.500]	HO	1.811	0.000	$\omega_{\mathrm{HO}} = 3945.580\ \mathrm{cm}^{-1}$, $M_{\mathrm{HO}} = 0.940$ AMU
u_1	SIN	50	[−0.900, 0.900]	GAUSS	−0.250	0.000	$W_{\mathrm{GAUSS}} = 0.100$
θ_2	WIGNER	45	$[0, \pi]$	WIGNER	—	—	$j_{\mathrm{ini}} = 0$, nosymm
ϕ	EXP	37	$[0, 2\pi]$	K	—	—	$m_{\mathrm{ini}} = 0$
α	EXP	15	$[0, 2\pi]$	K	—	—	$m_{\mathrm{ini}} = 0$

[a] Symbols of EXP, SIN, and HO stand for exponential, sine, and harmonic oscillator DVR, respectively, while symbol FFT denotes fast Fourier transform collocation. Symbol WIGNER denotes a three-dimension Wigner function as the basis function for angular coordinates θ_2, ϕ, and α.

[b] Symbols HO and GAUSS designate the choice of harmonic oscillator eigenfunction and Gaussian function, respectively, as 1D functions in building the guess wave functions for relaxations. Symbol EIGENF means eigenfunction of a specified potential which, in this work, is the 1D potential along r_1 setting z is sufficiently large (z_0 = 6.0 au) as to make the interaction between CO and Cu(100) negligible. Symbols WIGNER and K denotes associated 3D Wigner function and body-fixed magnetic quantum number, respectively, to specify the angular functions.

[c] In this cases only the position (that is 1.811 au) and frequency (that is 3945.580 cm^{-1}) parameters of the HO DVR are given, and then the ranges of the grids are calculated automatically.

TABLE II: Numerical details of the present MCCPD calculations[34,35]. The second column gives the method used in the present Monte-Carlo sampling. The third column gives the temperature ($k_{\mathrm{B}}T$ in eV) of each kind Metropols sampling. These samplings are distributed according to the weight $w = \exp(-V/(k_{\mathrm{B}}T))$, as given in Equations (12) and (13). The fourth and fifth columns present the numbers of the sampling points used for the fit and test, respectively. For constructing the CPD form of the PES, the combined set of sampling points of the distributions given in the `FIT` column (the fourth column) are used. The computation of the fitting error is performed for each temperature distribution individually, as given in the fifth column, the `TEST` column, where fit- and test-distributions are independent. The sixth and seventh columns give energy errors (in meV) between refitted and original potential using text sampling points, including their average (denoted by `MEAN`) and root-mean-square (denoted by `RMS`) values, respectively.

No.	Trajectory				Testing Error (meV)	
	Method	$k_{\mathrm{B}}T$ (eV)	FIT	TEST	MEAN	RMS
1	Metropolis	5.0×10^{-4}	3.0×10^{5}	2.0×10^{6}	2.79×10^{-1}	2.63
2	Metropolis	1.0×10^{-3}	3.0×10^{5}	1.0×10^{6}	7.65×10^{-1}	4.82
3	Metropolis	5.0×10^{-2}	2.5×10^{5}	1.0×10^{6}	-3.86×10^{-2}	2.56
4	Metropolis	5.0×10^{-1}	1.0×10^{5}	7.0×10^{5}	4.11×10^{-2}	11.57
5	Metropolis	1.0×10^{0}	5.0×10^{4}	1.0×10^{5}	1.87×10^{-1}	25.60
6	Metropolis	2.0×10^{0}	5.0×10^{4}	1.0×10^{5}	1.94×10^{-1}	28.42
7	Metropolis	4.0×10^{0}		5.0×10^{4}	7.05×10^{-2}	27.99
8	uniform		1.0×10^{5}	1.0×10^{6}	-3.95×10^{-1}	36.87
in total			1.15×10^{6}	5.95×10^{6}	1.23×10^{-3}	7.49

TABLE III: Excitation energies of the water molecule in the first excited ro-vibrational states (all energies in cm^{-1}) of the bond symmetry and asymmetry stretches (denoted by ν_1 and ν_3, respectively), the bond bending (denoted by ν_2). Here, we also given excitation energies for the vibrational excitations of the O-H bonds (denoted by ν_4 and ν_5) together with the frustrated rotations of the Euler angles for yaw, pitch, and roll rotations (associated with α, ϕ, and θ_2, respectively, as shown in Figure 1) of the BF coordinates set (denoted by ν_6, ν_7, and ν_8, respectively). These vibrational eigen-states will be the initial states of the concequence ML-MCTDH propagations. In these eigen-states the COM of the water molecule is located at z_0 = 6.0 au and hence the excitation energies of the frustrated rotations are very small. The first and second columns give the vibrational modes and corresponding symbols. The third column present the present 9D MCTDH relaxation results at z_0 = 6.0 au. For comparison, the previously reported excitation energies for the H_2O/Cu(111) system are also given in the fourth, fifth, and sixth columns. Excitation energies of the water molecule in the gae phase are also given in the other columns for comparison, where the electron structure calculations are performed by various methods in conjugation with the aug-cc-pVTZ basis set.

		Excitation Energies [a] (in cm^{-1})			Excitation Energies of H_2O (in cm^{-1})			
Mode	Symbol	MCTDH [b]	Zhang *et al.* [c]	Guo *et al.* [c]	B3LYP [b]	MP2 [b]	CCSD(T) [b]	Expt. [d]
symmetry stretch	ν_1	3520	3517	3437	3796	3822	3832	3802
bond bending	ν_2	— [e]	1545	1537	1627	1628	1646	1615
asymmetry stretch	ν_3	3624	3614	3526	3899	3948	3942	3694
O-H stretch	ν_4	3218						
O-H stretch	ν_5	3217						
yaw (α) rotation	ν_6	0.5						
pitch (ϕ) rotation	ν_7	4.2						
roll (θ_2) rotation	ν_8	25.4						

[a] These columns give excitation energies for the H_2O/Cu(111) system with z_0 = 6.0 au.

[b] This work.

[c] Results computed by Zhang and co-workers[6] and Guo and co-workers[1].

[d] See also Reference[42].

[e] In this work, the bond angle θ_1 was transferred to $u_1 = \cos\theta_1$ and thus the excitation of ν_2 will not be considered.

FIGURE CAPTIONS

Figure 1: The schematic diagram of the body-fixed (BF) coordinates set of the water molecule, where $\vec{r}_1$ is the vector from the O atom to the first H atom, $\vec{r}_2$ the vector from the center of mass (COM) of OH, $G_{\rm OH}$, to the second H atom, $\theta_1 \in [0, \pi]$ the angle between the $\vec{r}_1$ and $\vec{r}_2$ vectors. The z axis of the BF frame, $z^{\rm BF}$, is parallel to $\vec{r}_2$. The $(x^{\rm BF}, z^{\rm BF})$ half plan with $z \geq 0$ is determined such that $\vec{r}_1$ is parallel to this half plan. The origin of the BF frame is, in principle, the COM of the water molecule but the origin of the frame has no impact on the definition of the angles and distances.

Figure 2: The schematic diagram of the space-fixed (SF) coordinates set of the water molecule, where the axes of the SF frame are parallel to the laboratory-fixed (LF) frame. The origin of the SF frame is the COM of the water molecule, where $\theta_2 \in [0, \pi]$ and $\phi \in [0, 2\pi)$ are the spherical coordinates of $\vec{r}_2$ in the SF frame. The H′ atom is the projection of the top of $\vec{r}_2$ onto the $(x^{\rm SF}, y^{\rm SF})$ plan.

Figure 3: The ML-MCTDH wavefunction structure (ML-tree structure) for the 9D quantum dynamcis of the surface scattering of H_2O on the Cu(111) surface, where H_2O collides on Cu(111) and then reflects back or dissociates to the H and OH fragments. The maxima depth of the ML-tree is five layers and the first layer separates the three coordinates of the H_2O COM from the coordinates of the inner motions of H_2O. The number of SPFs for each layer are also given. The numbers of primitive basis sets to represent SPFs of the deepest layer are given next to the lines connecting with the squares (see also Table I).

Figure 4: The reduced densities of the 2D wave functions on the r_1-r_2 plane, together with the contour plots of the PES. The left and right panels give those for the symmetry and asymmetry stretch modes, respectively. These wave functions are used as initial wave functions in 9D ML-MCTDH calculations for mode-specific dynamics of H_2O/Cu(111). The energies of these vibrational states can be found in Table III.

Figure 5: Same as Figure 4, except for the states of O-H bond excitation-specific modes. The

left and right panels give reduced densities of the 2D wave functions on the z-r_1 and z-r_2 planes, respectively, together with the contour plots of the PES. These eigen-states are used as initial wave functions in 9D ML-MCTDH calculations for bond excitation-specific dynamics of H_2O/Cu(111). The energies of these vibrational states can be found in Table III.

Figure 6: Dissociative sticking probabilities versus collision energy (in eV) computed for the 9D model with rigid surface atoms. The black, red, and blue lines represent the dissociation probabilities when the water molecule is initially in the ground state (denoted by "GS"), symmetry excited state (denoted by "symm. mode"), and asymmetry excited state (denoted by "asymm. mode"). The green and yellow lines represent those where the water molecule is in the excited states associated with the r_1 and r_2 coordinates, which are denoted by "r1 excitation" and "r2 excitation", respectively. The brown, purple, and crimson lines represent those where the water molecule is in the excited states associated with the angular coordinates.

Figure 7: Comparsion of the time-dependent expectation values of the total energy of the water molecule from the 9D model, that is $\langle E(t)\rangle = \langle\Psi(t)|H|\Psi(t)\rangle$, where H is the Hamiltonian operator of the H_2O/Cu(111) system. The colored lines represent the results computed by various excited states and are illustrated by the same color scheme as in Figure 6. Here, the propagation time is cut at 450 fs.

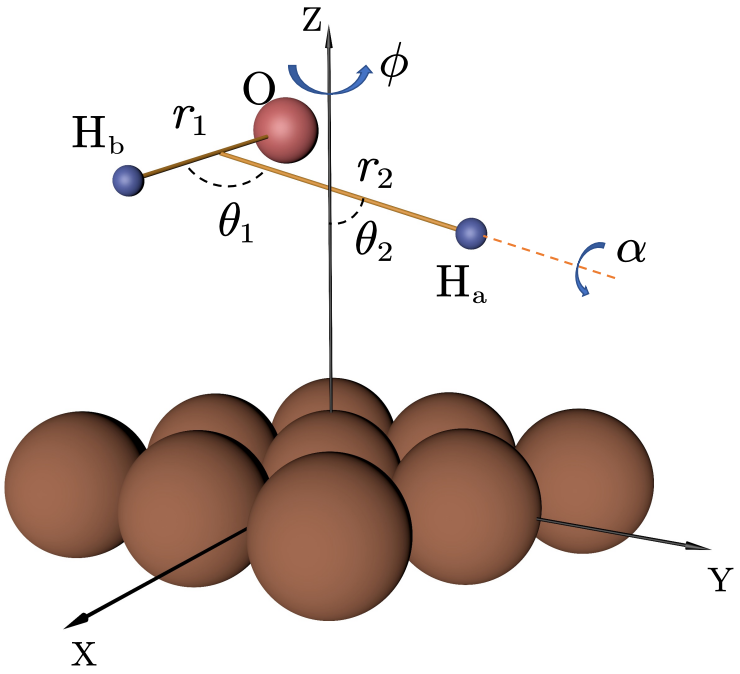

FIG. 1: wat-Cu111, MCCPD, ML-MCTDH

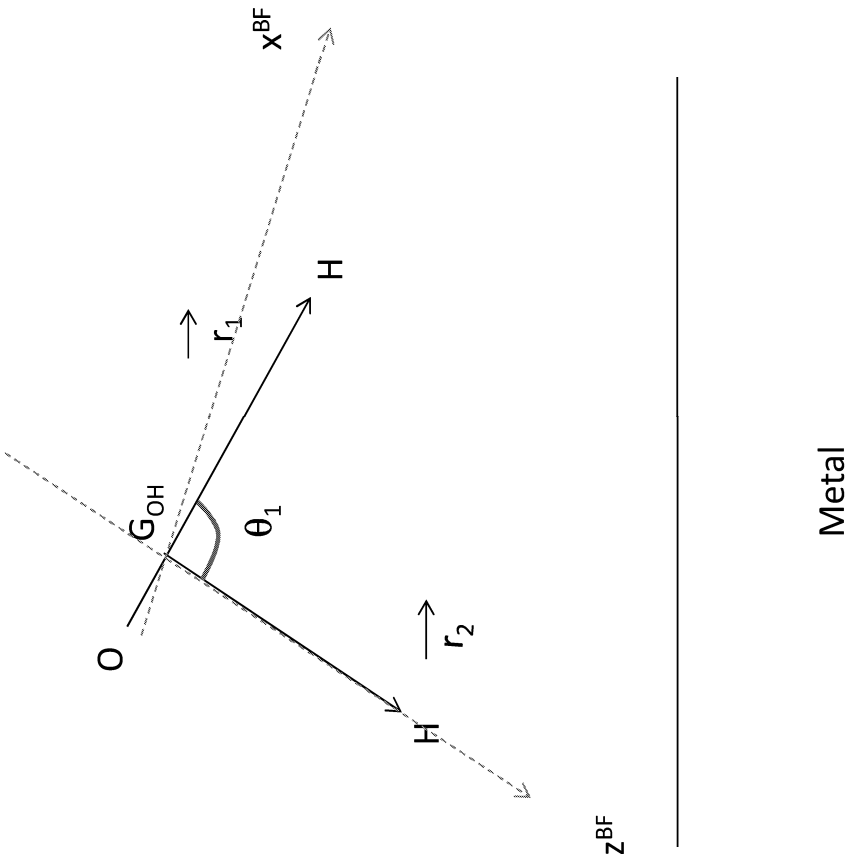

(a) The BF frame in the present work

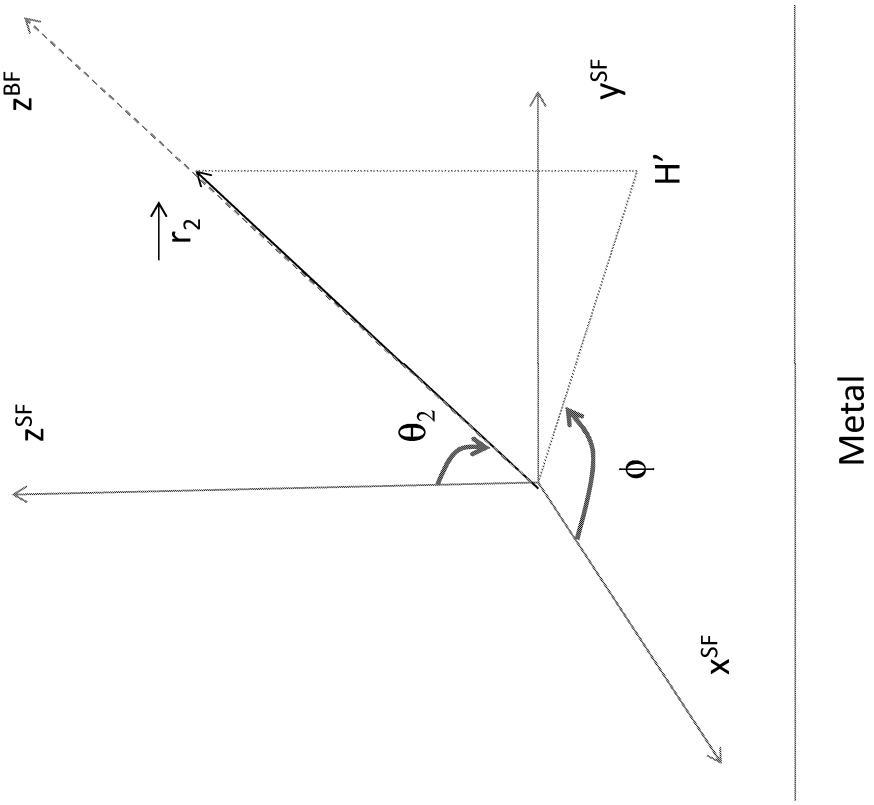

(b) The SF frame in the present work

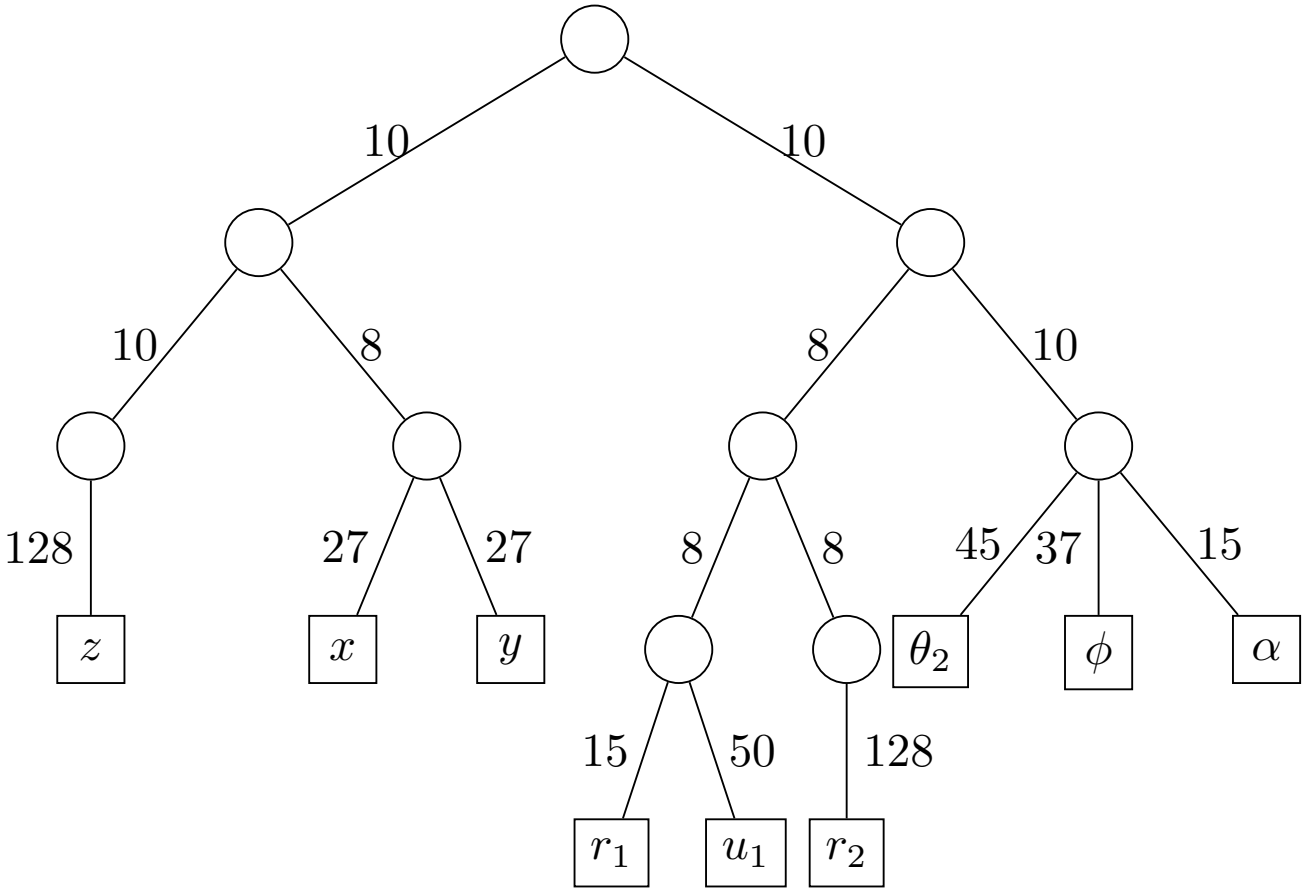

FIG. 3: wat-Cu111, MCCPD, ML-MCTDH

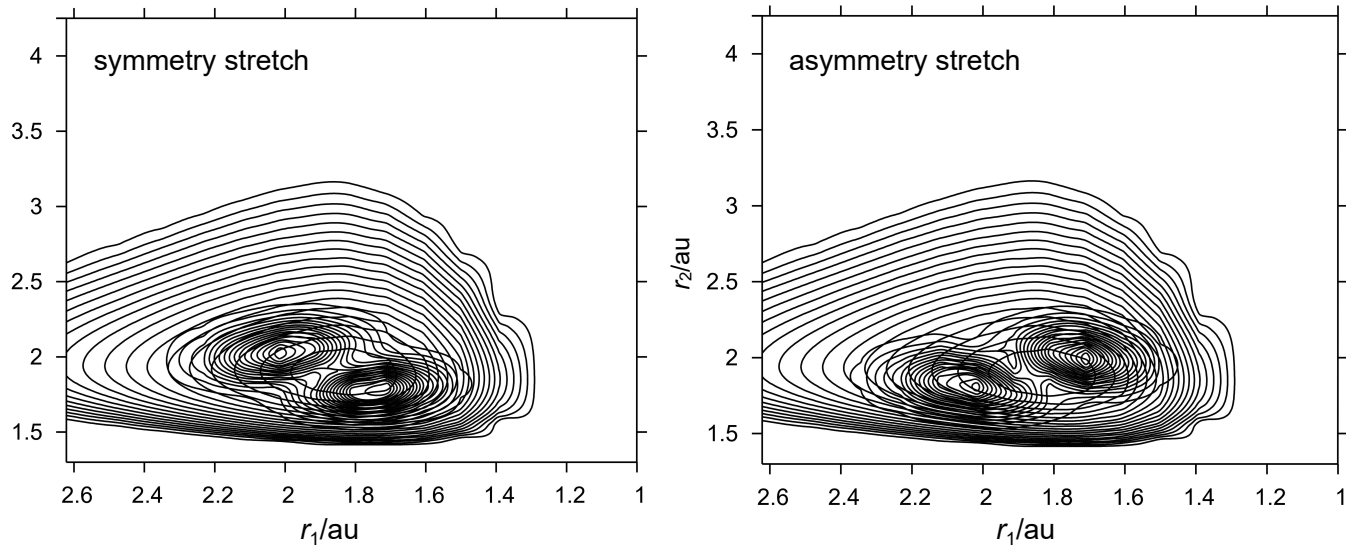

FIG. 4: wat-Cu111, MCCPD, ML-MCTDH

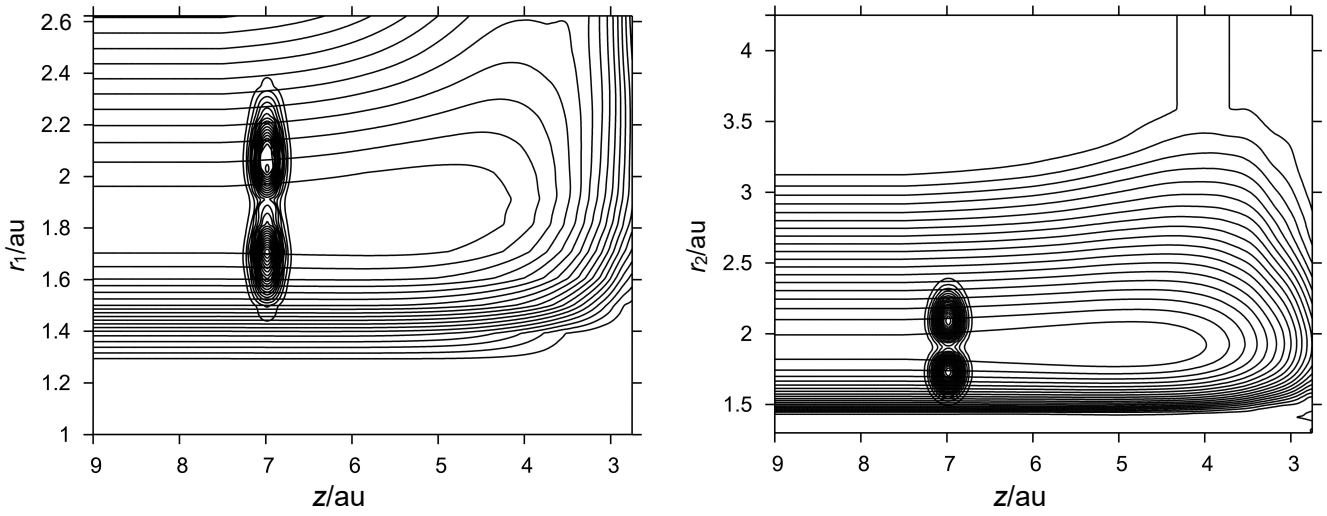

FIG. 5: wat-Cu111, MCCPD, ML-MCTDH

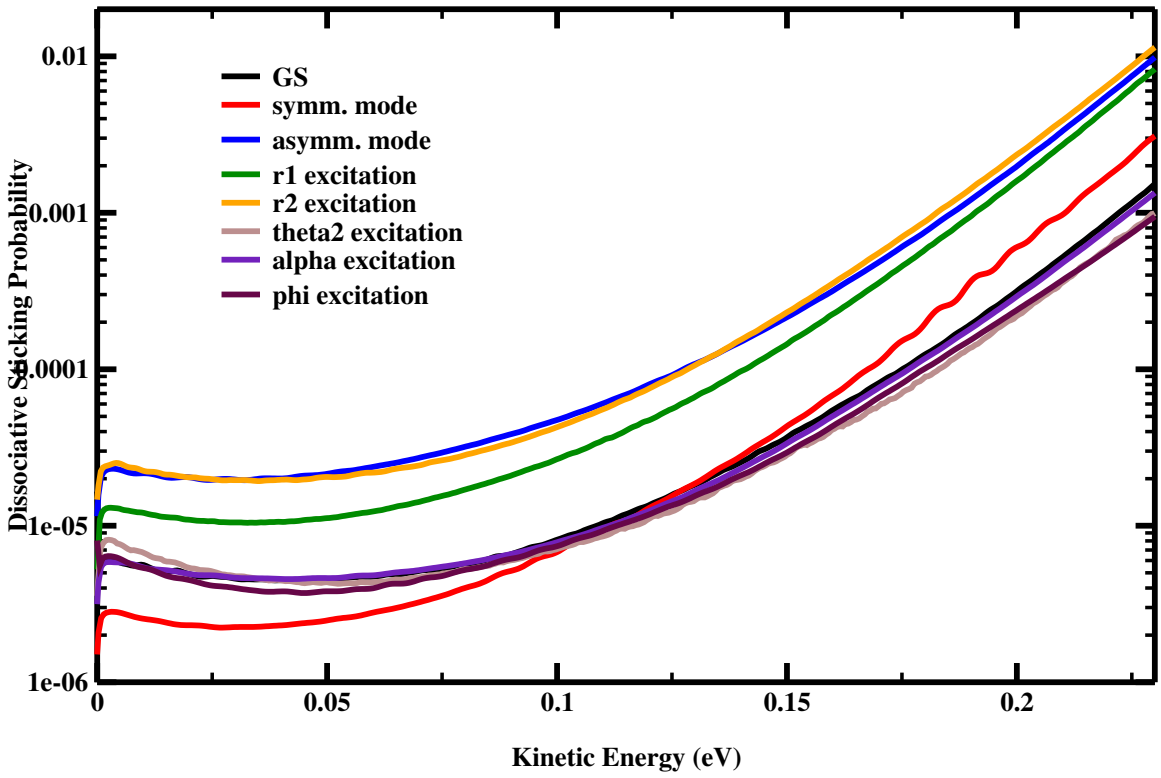

FIG. 6: wat-Cu111, MCCPD, ML-MCTDH

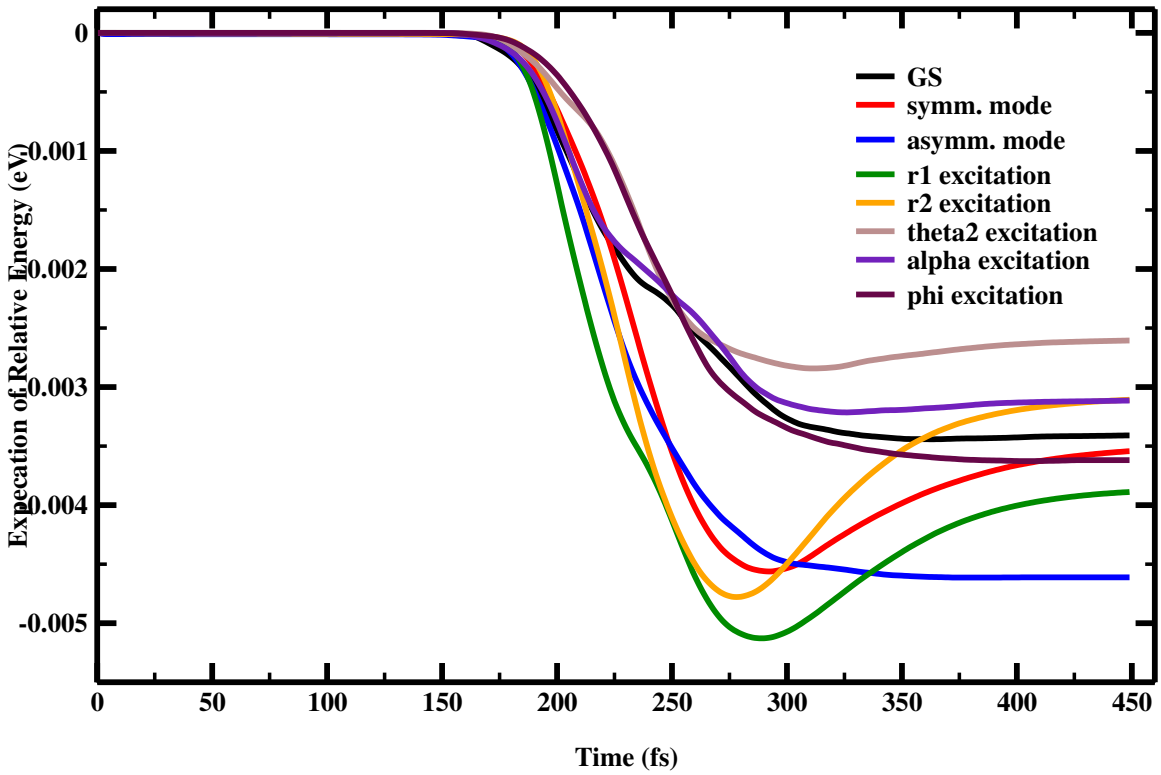

FIG. 7: wat-Cu111, MCCPD, ML-MCTDH